Fabricating a novel HLC-hBMP2 fusion protein for the treatment of bone defects

Zhuoyue Chen[a], Zhen Zhang[a], Zhaoyue Wang[a], Jiawei Wu[a], Yihang Wang[a], He Si[a],

Xin Xie[a], Lijun Shang[*b], Daidi Fan[*c], Fulin Chen[*a]

[a] Provincial Key Laboratory of Biotechnology of Shaanxi; Key Laboratory of Resource Biology and Modern Biotechnology in Western China; Faculty of Life Science, Northwest University, 229 TaiBai North Road, Xi'an, Shaanxi Province 710069, P.R. China.

[b] School of Human Sciences, London Metropolitan University, London, N7 8DB, UK.

[c] Shaanxi Key Laboratory of Degradable Biomedical Materials; Shaanxi R&D Center of Biomaterial and Fermentation Engineering; School of Chemical Engineering, Northwest University, 229 TaiBai North Road, Xi'an, Shaanxi Province 710069, P.R. China

* E-mail: l.shang@londonmet.ac.uk; fandaidi@nwu.edu.cn; chenfl@nwu.edu.cn

ABSTRACT

Treating serious bone trauma with an osteo-inductive agent such as bone morphogenetic proteins (BMPs) has been considered as an optimized option when delivered *via* a collagen sponge (CS). Previous work has shown that the BMP concentration and release rate from approved CS carriers is difficult to control with precision. Here we presented the fabrication of a recombinant fusion protein from recombinant human-like collagen (HLC) and human BMP-2 (hBMP2). The fusion protein preserved the characteristic of HLC allowing the recombinant protein to be expressed in *Yeast* (such as *Pichia pastoris* GS115) and purified rapidly and easily with mass production after methanol induction. It also kept the stable properties of HLC and hBMP2 in the body fluid environment with good biocompatibility and no cytotoxicity. Moreover, the recombinant fusion protein fabricated a vertical through-hole structure with improved mechanical properties, and thus facilitated migration of bone marrow mesenchymal stem cells (MSCs) into the fusion materials. Furthermore, the fusion protein degraded and released hBMP-2 *in vivo* allowing osteoinductive activity and the enhancement of utilization rate and the precise control of the hBMP2 release. This fusion protein when applied to cranial defects in rats was osteoinductively active and improved bone repairing enhancing the repairing rate 3.5- fold and 4.2- fold when compared to the HLC alone and the control, respectively. There were no visible inflammatory reactions, infections or extrusions around the implantation sites observed. Our data strongly suggests that this novel recombinant fusion protein could be more beneficial in the treatment of bone defects than the simple superposition of the hBMP2/collagen sponge.

Keywords

Fusion protein, human-like collagen, human bone morphogenetic proteins-2 (hBMP-2), controllable release, osteogenic activity

1. Introduction

Treating serious bone trauma is a clinical challenge and always requires the assist of osteo-inductive agents such as bone morphogenetic proteins (BMPs) [1]. BMPs normally provide a primordial signal for osteoprogenitor cells to differentiate into osteoblasts and then to form the bone extracellular matrix (ECM) [2] while BMPs retain at the site of injury and render an initial support which allows cells to attach and further regenerate the lost architecture on the ECM [3]. More than 20 types of BMPs have now been cloned, and BMP-2 and BMP-7 have the strongest osteogenic activity and are the most effective osteogenic factors [4-6]. However, BMP-2 is a water-soluble protein and easily diffused (the half-life is only 7~16 minutes [7]) after being implanted into a defect site, resulting in low osteogenic efficiency. Normally a carrier system that can load with BMP-2 in an appropriate low dose and with a sustained release profile is substantially needed [8-15].

Collagen, being the most abundant protein in mammalian connective tissue and the main non-mineral component of bone, can gradually degrade, has good biocompatibility, and can be easily molded into porous materials. Collagen has been a good candidate to release a growth factor slowly [16]. Animal collagen used as a sustained release carrier for BMP-2 can prolong the release time of BMP-2 and enhance the osteoinductive activity of BMP-2, thereby improve the bone repairing [17-23]. However, the methods used to combine BMP-2 with collagen are mainly through soaking collagen in BMP-2 solution [17-22]. Due to the low affinity of growth factors and collagen [24], the release rate of BMP-2 is difficult to control and the utilization of BMP-2 is incomplete. In addition, animal-derived collagens have potential viral risk and immunogenicity [25]. Therefore, designing a novel safer carrier with low immunogenicity and precise control of BMP-2 release is the key to improve the BMP-2 utilization for bone repairing.

The human-like collagen (HLC) is a recombinant protein and obtained by genetic engineering on the basis of a natural human collagen repeat sequence of "Gly-Pro-Hyp",

"Gly-Pro-Xaa" or "Gly-Xaa-Yaa" (Xaa, Yaa represents one random amino acid) [26]. HLC keep the properties of the natural collagen with the advantages of high porosity, high elastic modulus, good processing performance, no viral risk and low immunogenicity, and have been widely studied in hemostatic sponge [26], skin injury treatments [27], and tissue engineering vascular scaffolds [28]. We recently used glutamine transaminase (TG) to enzymatically cross-link this HLC to obtain a specially structured HLC sponge with enhanced mechanical strength and vertical pore structure, and then loaded this HLC with BMP-2 to repair bone. Although the new HLCs, which can now be mass-produced in our lab, overcome limitations of commercially available animal-derived collagens as a delivery system for bone repairing, the release rate of BMP-2 through this HLC delivery system is still difficult to control and the rapid release of a higher dose of BMP-2 (*i.e*, 5μg) could even induce the bone hyperplasia [29].

In this study, we fabricated a novel fusion protein using the recombinant HLC as a carrier for hBMP2 to address the above-mentioned concerns. This fusion protein was expressed in *Pichia pastoris* GS115, purified and mass-produced. The structure and properties of this fusion protein were furthered tested by scanning electron microscope (SEM), mechanical analysis, swelling behavior analysis, enzymatic degradation and cellular assessment assays. A cranial defect animal model was then used to test the effectiveness of this novel recombinant fusion protein. The novel fusion protein fabricated in this study greatly extend the ability of HLC in loading and releasing BMP-2 and would be beneficial in the treatment of bone defects, and the methods developed in this study could also release other growth factors and be used in other medical applications.

2. Materials and methods

2.1. Design of the HLC-hBMP2 fusion protein

To develop the HLC-hBMP2 fusion protein for controllable release of hBMP-2 and with osteogenic activity in bone defect repairing, the modified gene code of the human collagen type I (Col I) was used, synthesized and linked with the hBMP-2 gene. Then *Pichia pastoris* GS115 was transformed by the plasmid with HLC-hBMP2 gene and the HLC-hBMP2 fusion protein was then obtained through fermentation of yeast. In order to ensure that the BMP-2 and the HLC were not affected by a steric hindrance from each other and can be freely folded, a linker peptide rich in small molecule amino acids such as $(G)_n$, $(GGGGS)_n$, (n=1-4) was designed between the HLC and the hBMP2. Structures of the designed fusion proteins were obtained through the I-TASSER server (https://zhanglab.ccmb.med.umich.edu/I-TASSER/). From all designed proteins, we chose one HLC-hBMP2 sequence in which the hBMP2 active site was fully exposed (Fig. 1). In this study, we compared this novel fused protein with both the recombinant HLC and the HLC sponge absorbed hBMP2 through glutamine transaminase (TG) link in our previous work [29].
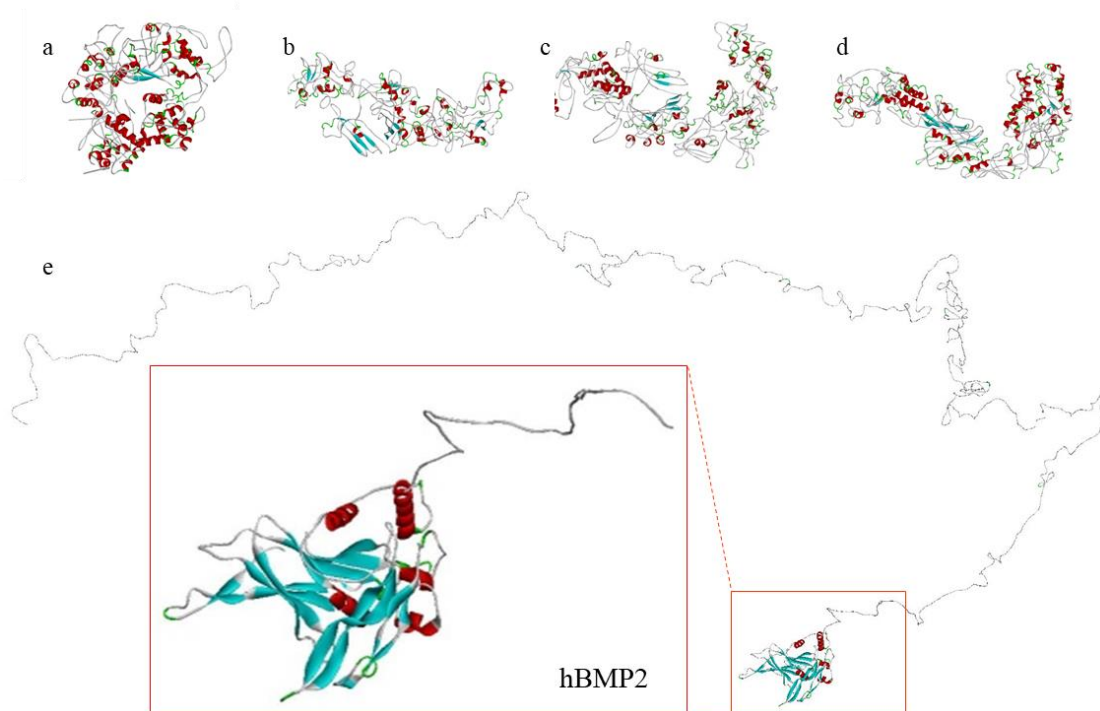

Fig. 1. Tertiary structure prediction of HLC-hBMP2 fusion protein with different connecting peptide. (a) Spherical protein conformation enveloping the hBMP2 active site; (b-d) Two proteins interfering with each other while folding; (e) hBMP2 connected

with the end at the spiral structure of HLC.

2.2. Construction of the HLC and the HLC-hBMP2 fusion protein expression plasmids

The gene sequence of HLC (Supporting Information-Sequence 1) with an *Xho* I site at the 5'-end and *Eco*RI site at the 3'-end was chemically synthesized. The HLC gene fragment was inserted between the *Xho* I and *Eco*RI sites at the sequence of the pPIC9K plasmid, thus the pPIC9K-HLC plasmid was constructed. Another structural gene for GGGGS-hBMP2 (Supporting Information-Sequence 2) with an *Eco*RI site at the 5'-end and *Not* I site at the 3'-end was also chemically synthesized. The GGGGS-hBMP2 gene fragment was then inserted between the *Eco*RI and *Not* I site at the sequence of pPIC9K-HLC. The gene expression plasmid (pPIC9K-HLC-hBMP2) for the HLC-hBMP2 fusion protein was then constructed. In order to verify whether the expression vector contained target fragments, the pPIC9K-HLC-hBMP2 plasmid was analyzed by digesting with *Xho* I and *Not* I. The gene sequencing of the pPIC9K-HLC-hBMP2 plasmid was tested.

2.3. Expression and purification of the HLC and the HLC-hBMP2 fusion protein

Plasmid pPIC9K-HLC-hBMP2 was linearized using *Sal* I and transformed into *Pichia pastoris* GS115 by electroporation (Elector Cell Manipulator, Bio-Rad, USA) at 1500V, 200Ω, 25μF, 0.2cm cuvettes. The high expression strain was selected using minimal dextrose (MD) medium plates containing 0.25, 0.5, 1.0, 2.0, 2.5, 3.0, and 4.0 mg/mL of G418, and then cultivated in the yeast extract peptone dextrose (YPD) medium overnight at 30℃ and 250rpm. The culture was transferred into the Buffered glycerol complex medium (BMGY) and further cultured at 30℃ and 250rpm until the OD 600 reached 2.0-8.0. After collected by centrifuging at about 4000 rpm for 3 min at 4℃, the cell pellets were diluted to an OD 600 of 1.0 in buffered methanol complex medium (BMMY). Methanol (0.5%) was added to the culture medium every day to induce

protein expression, and one ml medium was collected every day to check the expression level and to determine the optimal time to harvest the target protein.

The high expression strain was inoculated into fermenters (Shanghai Baoxing, 5L and 150L fermenters). The culture conditions and culture media in the fermentor were shown in Table S1. After 5 days of fermentation, the expression culture was collected and centrifuged at 4℃ for 30 minutes. The supernatant was then collected and detected by SDS-PAGE in order to identify the HLC-hBMP2 protein. After that, the cell fragments were removed from the supernatant containing the HLC-hBMP2 by the immersion hollow fiber membrane (Tianjin Membrane Technology Co., Ltd.), and subsequently desalted by a 10kD cut-off filter (Tianjin Membrane Technology Co., Ltd.). In the end, the HLC-hBMP2 with purity above 95% was obtained by an ion-exchange chromatography using an SPFF strong cation exchange column and AKTA purification system (GE, USA). At the same time, we used the same method to obtain the purified HLC as a control.

2.4. Preparation of the HLC and the HLC-hBMP2 scaffold

The HLC-hBMP2 fusion protein was a soluble protein. The EDC/NHS/MES system was used to cross-link HLC-hBMP2 to obtain an insoluble scaffold material of HLC-hBMP2. Firstly, HLC-hBMP2 fusion protein was dissolved in double-distilled water (2% w/v), immediately adding 0.1M EDC, 0.02M NHS, and 0.1M MES. The bubbles in the solution were removed by centrifugation after thoroughly blending, and then the solution was statically placed at 4℃ for 24 hours. Finally, the HLC-hBMP2 hydrogel obtained by cross-linking was vacuum freeze-dried and stored in a dryer for later use. The HLC scaffold was prepared as a control using the same method detailed as above.

2.5. Characterization of the HLC-hBMP2 scaffold

2.5.1. Morphological characterization

The general morphology of HLC-hBMP2 fusion material was obtained by a digital camera. The microscopic morphology of the HLC-hBMP2 fusion material was further observed by a scanning electron microscope (SEM, Hitachi s-4700, Japan).

2.5.2. Mechanical characterization

The mechanical properties of HLC and HLC-hBMP2 porous sponge materials were tested using a material testing machine (Instron-5542, Canton, MA, USA). The sample was made into a cylinder of 8mm diameter×5mm height, and the chuck was placed at a speed of 0.5mm/min to approach and compress the sample. The compression was stopped once the sample was irreversibly deformed. The elastic modulus of the HLC-hBMP2 porous sponge was calculated from the generated force and displacement curves.

2.5.3. Swelling behavior

The swelling behavior of HLC-hBMP2 fusion material was tested in simulated body fluid (PBS) according to the method of Parmar *et al.* [30] to evaluate its stability. The HLC was used as the control. Briefly, HLC and HLC-hBMP2 fusion materials (n=6) were weighed and recorded as dry weight (Wd). Then the materials were immersed into the PBS to form hydrogels. Subsequently, the formed hydrogels soaked in the PBS solution were taken out at 2, 4, 6, 24, and 48 hours, respectively. After further washing with PBS 2 to 3 times, the wet weight (Ws) of formed hydrogel was weighed and recorded. The calculation of the swelling ratio of the hydrogel was as follows:

$$\text{Swelling ratio} = \frac{W_S - W_d}{W_d}$$

2.5.4 Enzymatic Degradation Kinetics

Enzymatic degradation was normally used as an accelerated measurement of material degradation [31]. Because the designed HLC backbone was originated from Col I, we therefore firstly used the Type I collagenase to test the enzymatic degradation of the HLC and the HLC-hBMP2 *in vitro*. We used Type II and Type IV collagenases as the

control. *In vivo* enzymatic degradation evaluation of the HLC and the HLC-hBMP2 was carried out in the later part of the study.

Briefly, HLC and HLC-hBMP2 were made into cylinders of 8mm diameter×3mm height, approximate 30 mg per sample (n=6). Type I collagenase (100U/mL, Sigma), Type II collagenase (100U/mL, Sigma) or Type IV collagenase (100U/mL, Sigma) dissolved in PBS was added to sample according to 5 mg sample with 1 mL collagenase solution, respectively.   After the samples were incubated for 10, 30, 60, 120, 180 and 240 min at 37°C, the digestion mixture was centrifuged at 18,000g for 1 min, then 50μL of the digestion solution was collected and stored at -20°C for analysis. The protein concentration in the release was detected using a BSA kit and a UV-visible spectrophotometer (BioRad).

2.6. MSCs adhesion, proliferation and migration

2.6.1 MSCs Culture

Sprague Dawley (SD) rats (6-8 weeks old and 220-250g weight) were obtained from the animal holding unit, Northwest University. Bone marrow samples were harvested according to the project approval (No: ACUC2013015) by the Institutional Animal Care and Use Committee (IACUC), Northwest University. Bone marrow mesenchymal stem cells (MSCs) were obtained from the SD rats according to our previous studies [32, 33].

2.6.2 MSCs adhesion on the HLC-hBMP2

Cell adhesion on the surface of the material was examined to test the cytocompatibility of the material. Briefly, 1×10^6 MSCs were seeded into each HLC- hBMP2 scaffold and incubated for 4 hours respectively. After that, the specimens were rinsed with PBS, fixed with 2.5% glutaraldehyde, and dehydrated in an ethanol solution of gradient concentration (i.e., 30, 50, 70, 90 and 100% respectively). After critical point drying, the specimens were eventually coated with gold-palladium. They were then examined by SEM.

2.6.3 MSCs proliferation on the HLC-hBMP2

In addition to cell adhesion assay, cell proliferation on the surface of the material is a vital indicator for evaluating cell cytocompatibility. The main procedure was to place HLC-hBMP2 porous material in a 96-well plate, to seed around 2×10^3 cells on each material, and to determine the number of cells by CCK-8 kit at different time points after inoculation. Meanwhile, the PBS treatment group was used as the blank control, the HLC treatment group was used as the negative control. This experiment therefore tested whether the material could promote cell proliferation.

2.6.4 MSCs migration on the HLC-hBMP2

To further test whether the HLC-hBMP2 and the HLC material had differential effects on cells, we compared cell migration on the HLC-hBMP2 and the HLC. Briefly, 5×10^5 MSCs were seeded into each well of the 6-well plate with bottom coated with the HLC-hBMP2 and the HLC, respectively. After MSCs nearly covered the bottom of the well, they were continually incubated with the 0.5% FBS medium for 24 hours. Then a straight line was drawn at the bottom of the 6-well plate covered with MSCs using a 10-μL pipette tip. The wells were then washed 3 times with PBS until no removed and suspended cells were present. Images were recorded at 0, 1, 2, 3, 4 and 5 days, respectively for analysis. The average migration distance was calculated by measuring the migration area (A) and field of view height (h) using Image-J software. The migration distance was calculated using the following formula.

$$\text{Migration distance (μm)} = \frac{A_0 - A_t}{h}$$

2.7 Evaluation of bone repairing by micro CT

Twelve Sprague Dawley (SD) rats (6-8 weeks old and 220-250g weight) were randomly and evenly divided into three groups: the HLC-hBMP2 fusion protein group, the HLC group and the without implant group as the control group. In our previous work, we studied the bone repairing of the HLC sponge absorbed hBMP2 in the same *in vivo*

experiment [29]. To minimize the use of animals, we used the dataset obtained in that study to discuss and compare the bone repairing of the HLC-hBMP2 fusion protein in this study.

The brief surgery process was as following: Animals were anesthetized with isoflurane. The hairs were removed with the 8% sodium sulfide solution, and the skin was cut from the midline of the skull for 20 mm to reveal the skull. The cranial drill was used to create an 8mm diameter hole. Subsequently, the porous material (a disc of 8mm in diameter and 3mm in height, approximate 30 mg) was implanted into the defect site and the incision was sutured layer by layer.

After 8 weeks of implantation, the animals were sacrificed by inhalation of CO_2. The skulls of the rats were collected, and evaluation on the cranial defect repairing was performed by micro-CT (Y. Cheetah, YXLON, Germany). The scanning voltage was 80kV, the current was 50μA, and 3D reconstruction was performed at a resolution of 10μm (VG Studio, v2.2, Volume Graphics Inc. Germany). The bone volume fraction (BVF) was calculated through the bone volume (BV) divided by the collected tissue volume (TV). The repairing rate of the cranial defect was calculated through the BVF of the newly formed tissue divided by the BVF of the normal calvarium.

2.8 Evaluation of the new formed tissues

2.8.1 Testing the amount of Col I in the new formed tissues

The designed HLC backbone was originated from Col I and Col I was one of the main contents of the bone ECM. We therefore detected the amount of the Col I in the newly formed tissues. The animals were sacrificed 8 weeks after implantation surgery, and newly formed tissues were taken and frozen at -80℃ until analysis. Firstly, we milled the frozen tissue in liquid nitrogen to powder, and then added the RIPA lysate (Sigma, USA) to extract the total protein from the tissue. After quantification of the total protein in each tissue with the BCA kit (Thermo Scientific, USA), the same amount of the total protein was added to each well. Finally, the amount of the Col I in the total protein from

each tissue were measured using the Col I Elisa Kit (Abcam, USA).

2.8.2 Histological evaluation of the new formed tissues

The obtained newly formed tissues were fixed in 4% paraformaldehyde. After decalcification, 7μm thick paraffin sections were prepared and stained with Hematoxylin and eosin (HE) and Masson Trichrome Staining (MTS), and then they were photographed by optical microscope (VHX-5000, KEYENCE, Japan).

2.8.3 Testing bone marker proteins in tissues using immunofluorescence

To further evaluate the repairing of bone defects, the expression of bone marker proteins OPN and Runx-2 were detected in new bone tissues by immunofluorescence. Firstly, the sectioned samples were soaked in 0.1% Triton-X100 for 10 minutes, washed with PBS, and blocked with 5% goat serum. Secondly, an anti-OPN antibody (host: mouse, Novusbio, NB110-89062SS) and anti-Runx-2 antibody (host: rabbit, Abcam, ab114133) were incubated overnight at 4°C. Then they were washed with PBS, and incubated with fluorescently labeled anti-mouse (Alexa Fluor® 488-conjugated, Jackson, 715-545-151) and anti-rabbit (Alexa Fluor® 594-conjugated, Jackson, 715-585-152) secondary antibody, washed with PBS again, and stained with DAPI for 5 minutes. Finally, the sections were observed by a laser confocal microscope (FV1000; Olympus Corporation, Tokyo, Japan).

2.9 Statistical analysis

The data was processed utilizing the SPSS20.0 statistical software package. Multivariate data were compared by one-way analysis of variance (ANOVA), while t-tests were used for pairwise comparison between groups. The statistically significant difference was set at $p < 0.05$.

3. Results

3.1 Validation of HLC-hBMP2 expression vector

We have successfully constructed the pPIC9K-HLC-hBMP2 plasmids (Fig. 2a). To verify the expression vector for the HLC-hBMP2 chain, the pPIC9K-HLC-hBMP2 plasmids were cut with restriction enzymes *Xho* I and *Not* I at the two ends of the HLC-hBMP2 genes. Our results showed that the HLC-hBMP2 genes (band of 1619 bp) have been inserted into pPIC9K vectors successfully (Fig. 2b). Results of DNA sequencing also proved the exact connection of HLC-hBMP2 genes to the expression vector (Fig. S1).

Pichia pastoris GS115 competent cells was electro-transformed by the linearized pPIC9K-HLC-hBMP2 plasmid, and low copy to high copy screening was performed by G418 resistant YPD plates. Several single colonies were randomly picked from G418-resistant plates and shaken overnight in YPD medium. A small amount of bacterial extracting genome was used as a template, and the primers of hBMP-2 was used to verify whether the target gene was in the strain (Fig. S2). Six strains of yeast expression strains were selected and transferred to BMGY medium in turn and cultured in BMMY medium. The culture was stopped after methanol induction for 5 days, the supernatant was collected by centrifugation, and the proteins were separated by SDS-PAGE (Fig. 2c). As shown in Fig. 2c, all 6 selected strains expressed HLC-hBMP2 fusion proteins successfully (molecular weight 51kD). In order to fully verify that the collected protein was the HLC-hBMP2 fusion protein, the N-terminal sequencing of the collected protein was performed, and the result further verified that the collected protein was indeed the actual HLC-hBMP2 fusion protein (Fig. S3). Based on the above results, the HLC-hBMP2 fusion protein was successfully expressed in the constructed yeast expression strain after methanol induction.
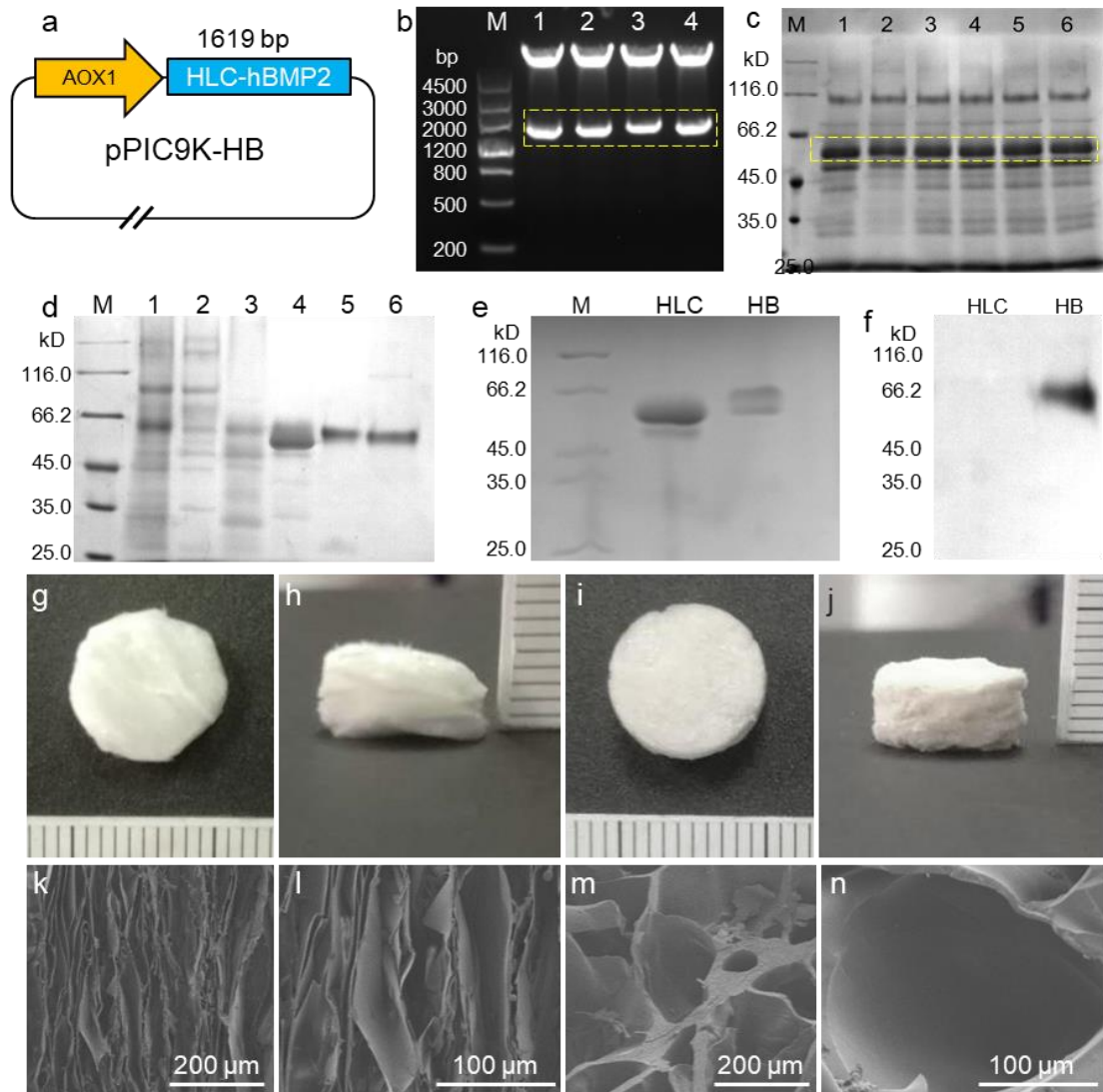
Fig. 2. HLC-hBMP2 produced by pPIC9K-HLC-hBMP2 plasmids in *Pichia pastoris* GS115 and the purification process. (a) Schematic diagram of the pPIC9K-HLC-hBMP2 plasmids; (b) Agarose gel electrophoresis of HLC-hBMP2 genes visualized by ethidium bromide staining. M: DNA Marker III (bp). lanes 1-4: Plasmids containing the HLC-hBMP2 genes digested with *Xho* I and *Not* I, producing a vector fragment (9.3 kb) and an HLC-hBMP2 gene fragment (1619 bp). (c) SDS-PAGE results showed that HLC-hBMP2 fusion protein (molecular weight 51kD) were expressed in all six strains of yeast. M: Protein marker (kD); lanes 1-6: the supernatant of the induced yeast. (d) the process of SPFF cation column purification of HLC-hBMP2 fusion protein shown in gel. M: Protein marker (kD); lane 1: the supernatant of fermentation fluid; lane 2: the post-column penetrating liquid; lane 3: the eluate after washing with

5% B phase (containing 1 M NaCl in citric acid buffer solution); lane 4: the eluate after washing with 10% B phase; lane 5: the eluate after washing with 15% B phase; lane 6: the eluate after washing with 100% B phase. (e) Comparison of the molecular weight of the HLC and the HLC-hBMP2 fusion protein by SDS-PAGE. (f) Western-Blot (using hBMP-2 antibody): lanes 1-2: purified HLC-hBMP2 fusion protein; lanes 3-4: purified HLC protein. (g-j): The general morphology observation of purified HLC (g, h) and HLC-hBMP2 (i, j): The material was a cylinder having a diameter of 10 mm and a height of 5 mm; (k-n): SEM morphology observation of the HLC and HLC-hBMP2 under different magnifications: (k) HLC and (m) HLC-hBMP2, magnified $200\times$; (l) HLC and (n) HLC-hBMP2, magnified $500\times$. The HLC was a layered porous structure, and the HLC-hBMP2 was a vertical through-hole structure by SEM.

3.2 HLC-hBMP2 expression and purification

The shaking flask culture resulted in the HLC-hBMP2 fusion protein expressed in the constructed yeast expression strain, and an amount of the targeted proteins was then obtained by high-density fermentation in a fermenter. After high-density fermentation, the supernatant of the fermentation fluid was collected, which contained the targeted HLC-hBMP2 proteins. Then the HLC-hBMP2 fusion protein was purified by SPFF cation column. Total protein in each purified step was shown in Fig. 2d. The first lane was the supernatant of the fermentation fluid after centrifuged and desalted, which contained lots of proteins. The second lane was the post-column penetrating liquid. Compared with the first lane, the band of about 51kD became lighter. This was due to that the target protein of 51kD size has been adsorbed on the cationic filler, and a large amount of the contaminants have passed through the column and flowed out. Lane 3 was the eluate after washing with 5% B phase (containing 1 M NaCl in citric acid buffer solution), where the target protein was less, and the contaminants with molecular weight was lower than the target protein elutes. Lane 4 was the eluate after washing with 10% B phase, where a great deal of the target protein was eluted, and the amount

of the contaminants was small. Lanes 5 and 6 were the eluates after washing with 15% B phase and 100% B phase, respectively. The purified target protein was seen in both Lane 5 and Lane 6 (Fig. 2d), but the volume of the eluate after washing with 100% B phase (Lane 6) was much less than that with 15% B phase (Lane 5). Therefore, we chose to collect the eluate after washing with 15% B phase and consequently obtained a large amount of the purified target HLC-hBMP2 fusion protein. Another reason for choosing the eluate after washing with 15% B phase was since the concentration of salts in 100% B phase was too high and made it too hard to desalt.

Comparing the molecular weights of HLC and HLC-hBMP2 fusion proteins, the HLC-hBMP2 fusion protein had slightly higher molecular weight than the HLC due to the fusion of hBMP-2 (Fig. 2e). The target protein was further detected by Western-Blot using hBMP-2 antibody. As shown in Fig. 2f, the purified HLC-hBMP2 fusion protein was observed on the membrane, however, the purified HLC did not show any band on the membrane. This result demonstrated that the target protein was HLC-hBMP2, which successfully fused with hBMP-2. At final product, the concentration of HLC-hBMP2 was 1 g purified proteins per 1L zymotic fluid from the 150L fermenter. This mass production of the fusion protein made it possible to explore its clinical application.

3.3 HLC-hBMP2 fusion protein fabricated a vertical through-hole structure with improved mechanical properties

3.3.1 Morphological characterization of HLC-hBMP2 scaffold

Both HLC and HLC-hBMP2 fusion proteins were soluble proteins. The morphology of HLC and HLC-hBMP2 after cross-linking with the EDC/NHS/MES system was shown in Fig. 2g-j. The material was prepared into a cylinder of 10mm in diameter and 5mm in height. The HLC and HLC-hBMP2 materials were all white and showed a porous sponge-like structure (Fig. 2g-j). The microstructure of the materials was observed by SEM. The HLC material had a lamellar porous structure (Fig. 2k, l), while the HLC-

hBMP2 fusion protein material was a vertical through-hole structure (Fig. 2m, n). The vertical pore size of porous material within the HLC-hBMP2 fusion protein was about 100μm (Fig. 2n), which was larger than the size of the MSC. This structure therefore was able to facilitate the migration of MSC into the material and the delivery of nutrients.

3.3.2 Improved mechanical characterization of HLC-hBMP2 scaffold

In order to explore the processability of HLC and HLC-hBMP2 porous materials, the elastic modulus of the two materials were measured with a versatile analyzer (Fig. 3a, b). The elastic modulus of HLC-hBMP2 (1.94 ± 0.11 MPa) was significantly higher than that of HLC material (1.72 ± 0.02 MPa, $p<0.05$, n=3). The structure changes of the material after HLC fused with hBMP-2 was visible (Fig. 2k-n), and HLC-hBMP2 showed vertical through-hole structure (Fig. 2m, n), which had better mechanical properties (Fig. 3a, b) than HLC (Fig. 2k, l) material itself.

3.4 HLC-hBMP2 fusion protein retained stable properties in the mimic body fluid environment and accelerated degradation in the enzymatic environment.

3.4.1 Swelling behavior

To evaluate if the property of HLC-hBMP2 was stable in the body fluid environment, the swelling ratio of the HLC and the HLC-hBMP2 fusion material after forming the hydrogel was further tested when they were immersed into the simulated body fluid for different times. As shown in Table S2, HLC and HLC-hBMP2 formed hydrogels after immersion in PBS for 24 h. The wet weight of the HLC and the HLC-hBMP2 hydrogel was 8.16 ± 0.60 times and 7.79 ± 1.85 times that of the dry weight before hydrogel formation, respectively. There was no statistical difference between the two ($p>0.05$, n=6). After the hydrogel was formed, the swelling ratio was stabilized for 2, 4, 6, 24, and 48 hours, and the swelling ratio curve turned to be stable with time (Fig. 3c). In

summary, both HLC and HLC-hBMP2 had high swelling ratio, strong water absorption and water retention capacity, and the swelling properties of the two materials were stable, and the swelling ratio tended to be stable with time.
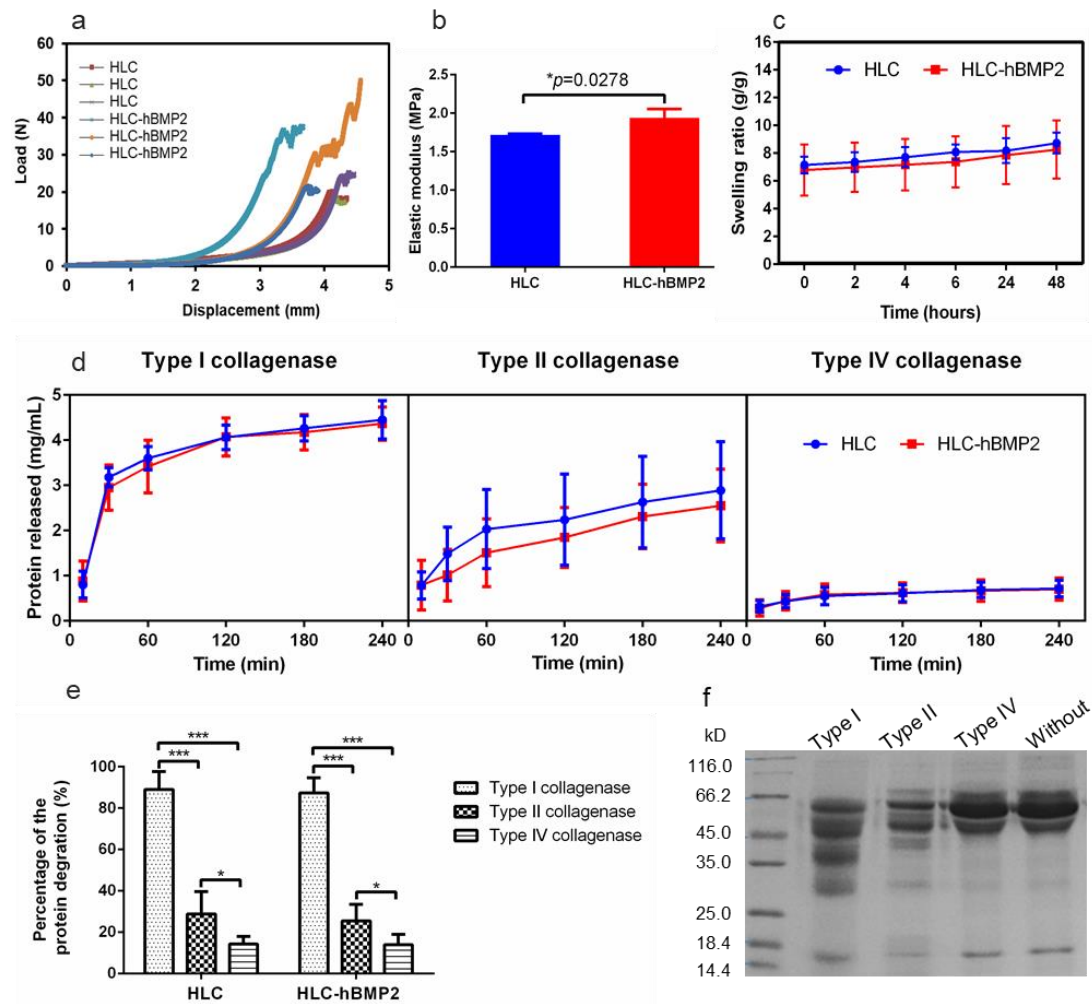

Fig. 3. Mechanical testing, swelling ratio and enzymatic degradation kinetics of the HLC and the HLC-hBMP2 fusion protein. (a) Compressed displacement-load curve; (b) Statistical results of elastic modulus (*p<0.05, n=3). (c) HLC and HLC-hBMP2 swelling ratio curve. The hydrogel swelling ratio testing was completed in PBS solution at pH=7.4, and HLC and HLC-hBMP2 were immersed in PBS for 24 hours to form a hydrogel. The swelling ratio of the hydrogel tended to be stable, and the swelling ratio of the two hydrogels at each time point showed no significant difference (p>0.05, n=6). (d) Enzymatic degradation kinetics demonstrated no difference in susceptibility between the HLC and the HLC-hBMP2 to all types of collagenases (p>0.05, n=6). (e)

The percentage of the HLC and the HLC-hBMP2 degradation was calculated according to the enzymatic degradation kinetics. Over 80% of the HLC or the HLC-hBMP2 were degraded in the Type I collagenase solution (100U/mL) within 4 hours (n=6). Compared with Type II collagenase or Type IV collagenase, the HLC and the HLC-hBMP2 were hydrolyzed significantly faster in the Type I collagenase solution (***p<0.001, n=6). The HLC and the HLC-hBMP2 were hydrolyzed faster in the Type II collagenase solution than that in the Type IV collagenase solution (***p<0.001, n=6). (f) SDS-PAGE of the HLC-hBMP2 in Type I, Type II and Type IV collagenase solution for 4 hours.

3.4.2 Accelerated degradation in the enzymatic environment

Digestion of materials in purified enzyme solution indicated that the HLC and the HLC-hBMP2 had equal susceptibility to all types of the collagenases (Fig. 3d) but most susceptibility to Type I collagenase (Fig. 3d-f). Notably, most of the HLC ($89.07\pm$ 8.56%, n=6) and the HLC-hBMP2 ($87.37\pm7.36\%$, n=6) were degraded in the Type I collagenase solution (100U/mL) within 4 hours. However, only $28.91\pm10.77\%$ of the HLC and $25.54\pm8.04\%$ of the HLC-hBMP2 were degraded in the Type II collagenase solution (100U/mL) within 4 hours. Compared with Type I or II collagenase, the less HLC ($14.38\pm3.65\%$) and the less HLC-hBMP2 ($14.01\pm4.93\%$) were degraded in the Type IV collagenase solution (100U/mL) within 4 hours (***p<0.001, n=6, Fig. 3e). The HLC and the HLC-hBMP2 were the fastest and most completely hydrolyzed in the Type I collagenase solution (***p<0.001, n=6, Fig. 3d, e). However, it is worth to note that *in vivo* degradation is cell-mediated, and thus enzyme susceptibility may not be a perfect predictor for material lifetimes *in vivo*.

3.5 HLC-hBMP2 fusion protein presented with good biocompatibility and enhanced MSCs migration

3.5.1 Adhesion and proliferation of MSCs on the HLC and HLC-hBMP2 materials

Fig. 4a-b showed the morphology of rat MSCs cultured on HLC (Fig. 4a) and HLC-hBMP2 (Fig. 4b) fusion protein materials after 4 hours. Pseudopods protruded from most of the MSCs on both materials, and some of the cells have spread out and formed a fusiform shape (Fig. 4a-b). These results demonstrated that both materials promoted the adhesion of MSCs. As shown in Fig. 4c, there was no significant difference on cell proliferation among the HLC, the HLC-hBMP2 group and the control group (MSCs cultured in the cell culture plate; $p>0.05$, n=12). These results demonstrated that the HLC-hBMP2 had as good biocompatibility and no cytotoxicity as the HLC.

3.5.2 Migration of MSCs on the HLC and the HLC-hBMP2 materials

The rat MSCs migration on the HLC and the HLC-hBMP2 materials were quantified. The MSCs migration on the HLC (Day 1: 169.48 ± 62.20 μm; Day 2: 260.69 ± 70.43 μm; Day 3: 414.74 ± 61.68 μm, n=12) and the HLC-hBMP2 (Day 1: 174.29 ± 56.25 μm; Day 2: 274.55 ± 67.08 μm; Day 3: 428.89 ± 58.88 μm, n=12) had no significant difference at the beginning of the assay ($p>0.05$, n=12, Fig. 4d) until day 4. Compared with the HLC (509.64 ± 79.70 μm, n=12), the HLC-hBMP2 was more permissive to MSCs migration at day 4 (585.25 ± 94.98 μm, $p<0.05$, n=12, Fig. 4d). This result showed that the HLC-hBMP2 enhanced MSCs migration in the new fabricated structure. There was no significant difference between HLC (623.04 ± 71.33 μm, n=12) and HLC-hBMP2 (624.29 ± 86.21 μm, $p>0.05$, n=12, Fig. 4d) at day 5 because cells had fully covered the space of the cell culture plate after migration for 5 days.

BMP2 is not only osteogenic but osteoinductive suggesting that it should drive MSC proliferation. However, BMP-2 cannot be released from the HLC-hBMP2 fusion protein without collagenase participation in our *in vitro* experiment. Therefore, HLC-hBMP2 fusion protein didn't promote the proliferation of MSC in this *in vitro* assay.
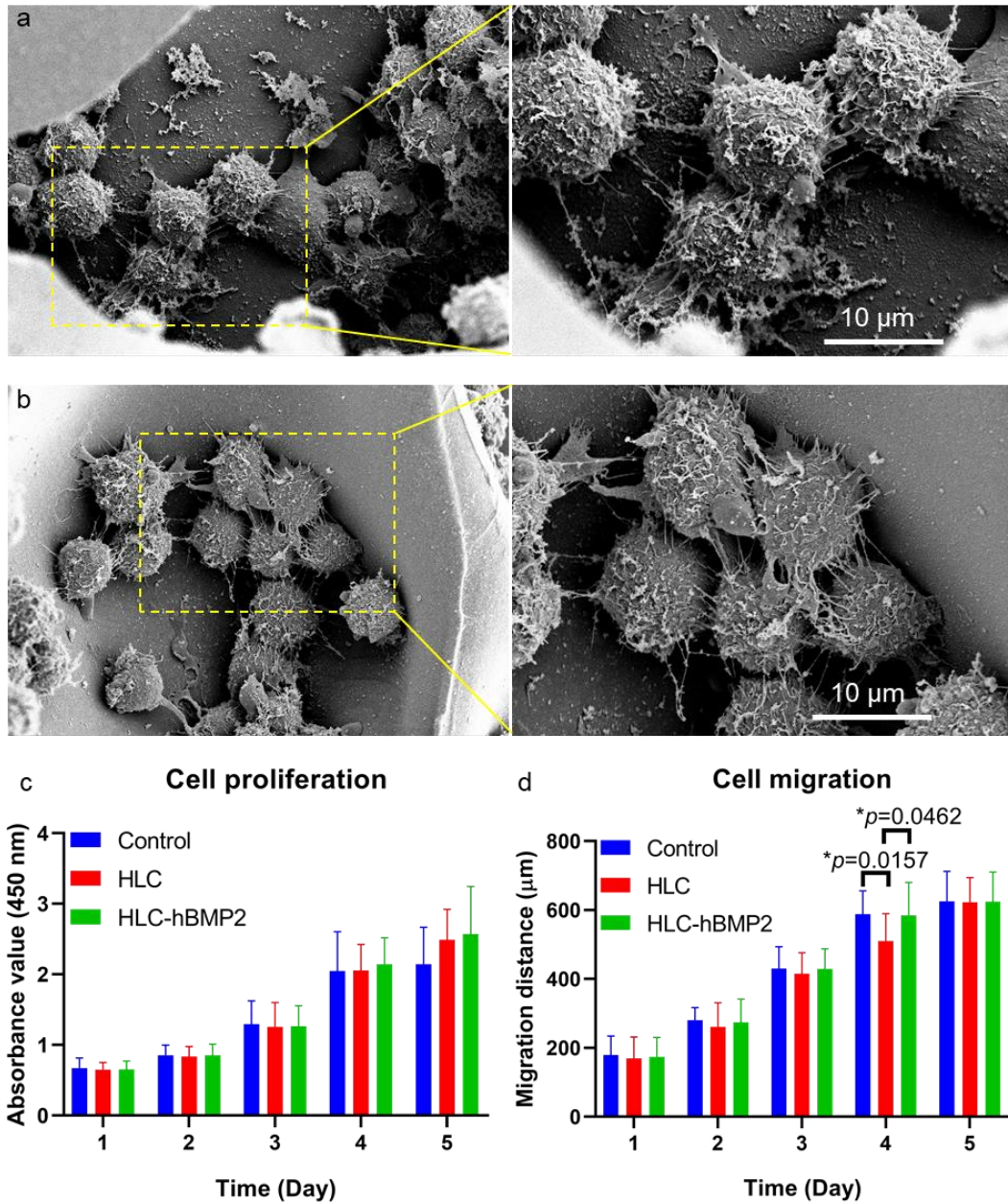
Fig. 4. Adhesion, proliferation and migration of rat MSCs on the HLC and the HLC-hBMP2 materials. (a-b) The morphology of MSCs cultured on (a) HLC and (b) HLC-hBMP2 fusion protein materials for 4 hours; scanning electron microscope magnification: 1.5k (left) and 3k (right); (c) Proliferation assay: There was no significant difference on cell proliferation among the HLC group, the HLC-hBMP2 group and the control group (rat MSCs cultured in the cell culture plate; $p>0.05$, $n=12$). (f) Migration assay: The migration distance of rat MSCs cultured on the HLC-hBMP2 for 4 days was significantly higher than that of rat BMSCs cultured on the HLC ($p<0.05$,

n=12). There was no significant difference between the HLC-hBMP2 group and the control group on the migration of MSCs at all-time points (rat BMSCs cultured on cell culture plates as the control; p>0.05, n=12).

3.6 HLC-hBMP2 fusion protein improved cranial defects repairing in SD rats with controlled hBMP2 release

3.6.1 Evaluation of bone repairing by micro CT

The rat cranial critical size defect repair model was used in this study to investigate the effects of the HLC-hBMP2 on the bone regeneration *in situ* as previously described [29]. All rats survived and showed no inflammatory reactions and infections for the period of 8 weeks. The repairing of rat cranial defects was observed by micro-CT at the end of 8 weeks. After implantation of HLC-hBMP2, the repairing rate of the cranial defects in SD rats was significantly improved than that in both the non-implanted material group and the HLC material group (Fig. 5a-d). As shown in Fig. 5a-c, at 8 weeks post operation, a small amount of bone tissue was visible along the edge of the defect in the control group (non-implanted material) and the HLC group, while a large amount of bone tissue was regenerated both at the edge of the defect and in the central region in the HLC-hBMP2 group. The micro-CT results showed (Fig. 5d) that after implantation for 8 weeks, the bone defect repair rate (51.72 ± 16.68%, n=4) in the HLC-hBMP2 group was significantly higher than that in the HLC group (21.01 ± 14.11%, p<0.05, n=4) and the control group (13.63 ± 3.62%, p<0.01, n=4). There was no significant difference in bone defect repair rate between the HLC group and the control group (p>0.05, n=4). These results indicated that the HLC alone can promote bone defect repairing, but its repairing ability was limited. The HLC alone was not able to repair large-size bone defects, while the HLC-hBMP2 had the ability to repair large-size bone defects (Fig. 5a-d). In addition, this recombinant fused HLC-hBMP2 had no side effects and safer for the bone repairing compared with other HLC sponge delivery

as evidenced in our previous work [29] where TG linked HLC loaded with 5 µg rhBMP-2 was implanted into the same rat cranial defect repair model but serious bone overgrowth was introduced the for 8 weeks (Fig. 8 in [29]).

3.6.2 Col I in the new formed tissues

Because the designed HLC backbone was originated from Col I, the composition and the structure of the HLC were almost the same as Col I. It is also well known that the Col I is one of the main contents of the bone ECM. In order to examine the degradation of the HLC and the HLC-hBMP2 *in vivo*, we therefore examined Col I in the newly formed tissues after implantation 8 weeks.

The amount of Col I detected in the new formed tissues was significantly higher from the HLC group (460.48 ± 196.90 ng/mL) than that from the control group (193.06 ± 63.91 ng/mL, $p<0.05$, n=4, Fig. 5e). While the amount of Col I from the HLC group was significantly less than that from the HLC-hBMP2 group (1033.12 ± 296.71 ng/mL, $p<0.05$, n=4, Fig. 5e). These results demonstrated indirectly that the HLC-hBMP2 significantly improved bone repairing. High-resolution images with high magnifications (Supplement Figures 5-10) further demonstrated that chondrocytes and osteoclasts were clearly visible in the newly formed tissue.

Our previous results indicated that the bone volume of the new formed tissues had no significant difference between the HLC group and the control group ($p>0.05$, n=4, Fig. 5d) using the micro CT. This was slightly different from the above Col I Elisa testing results (Fig. 5e). The reasons for this difference might be: (i) the HLC was not completely degraded after 8 weeks implantation, which contributed to the little amount of the Col I detected; (ii) the Col I Elisa testing might reflect the bone formation more sensitively than the micro CT did. Nevertheless, the amount of Col I detected from the HLC-hBMP2 group demonstrated the effectiveness of this new material in bone repairing.
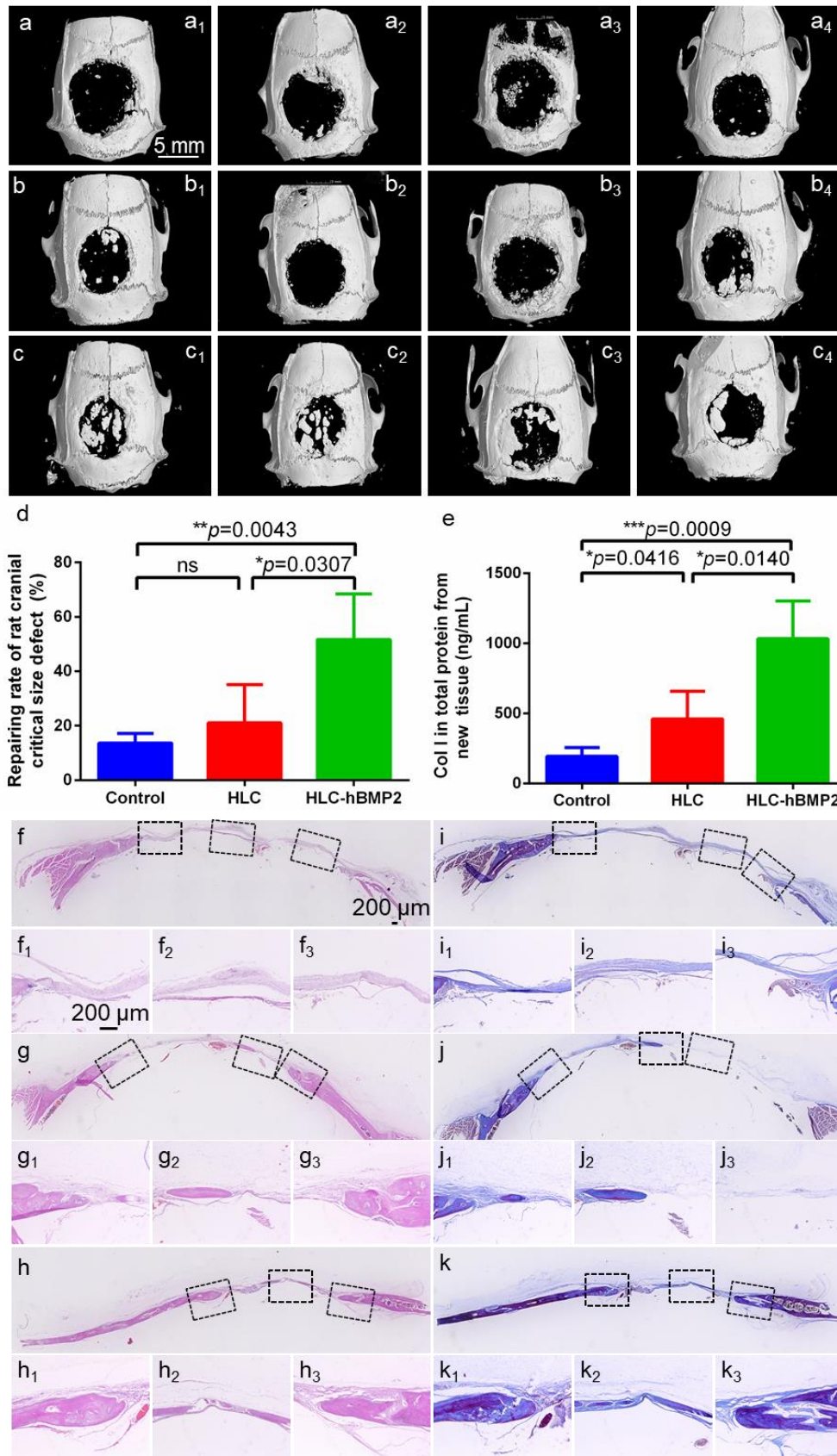
Fig. 5. Analysis of the newly formed tissues. Micro-CT scan, Col I detection and Histological analysis of the HLC and the HLC-hBMP2 porous materials implanted into

SD rats with critical size defect (8mm diameter defect) after 8 weeks. Micro-CT scan of (a) non-implanted material, (b) implanted HLC and (c) implanted HLC-hBMP2; (d) Repairing rate. After implantation of the HLC-hBMP2, the repairing rate of cranial defects in SD rats was obviously improved than that in the non-implanted material group and the HLC material group (*p<0.05, **p<0.01, n=4). (e) The amount of Col I detected in the newly formed tissues was significantly higher from the HLC-hBMP2 group than that from the control group (***p<0.001, n=4) or the HLC group (*p<0.05, n=4). While the amount of Col I detected in the newly formed tissues from the HLC group was significantly higher than that from the control group (*p<0.05, n=4). HE stain of (f) the control group (non-implanted material); (g) the HLC group; (h) the HLC-hBMP2 group, and MTS of (i) the control group (non-implanted material); (j) the HLC group; (k) the HLC-hBMP2 group. Three different repaired defect sites were chosen from all groups and labelled as 1-3 from left to right. The zoomed-out of chosen parts were shown below accordingly.

3.6.3 Histological and immunofluorescence evaluation of new formed tissues

After the implantation of the samples in the rat skull defect model, we observed its repairing effects for various time periods, including a shorter time scale of 2 weeks and 4 weeks, but no significant changes were observed in these early period times after surgery. The significant difference only appeared till after 8 weeks of implantation. At 8 weeks post operation, the samples of repaired tissues from all groups were analyzed by histochemistry. The osteogenesis of the new tissue formed from all groups at the defect site was observed by HE stain (Fig. 5f-h) and MTS (Fig. 5i-k). The results showed that only a thin layer of fibrous tissue in the defect site was formed in the control group (Fig. 5f, i). In the HLC group, a small amount of bone tissue was formed in the middle of the defect site (Fig. 5g, j). While in the HLC-hBMP2 group, continuous new bone tissue was formed in nearly all defect sites and many collagens were observed. In addition, the HLC-hBMP2 material has completely degraded (Fig. 5h, k).

Runx-2 is a transcription factor related to mesenchymal commitment to the osteogenic lineage. Runx-2 is also a preosteoblast marker [34] which could be detected in the early stage of stem cell differentiation to osteogenesis. Due to the slow releasing of the BMP-2 from our novel device HLC-hBMP2 in this study, the defect areas have not been completely repaired at the 8th week after intervention, so we inferred that the stem cell differentiation to osteogenesis could have still been happening in the defect site after 8 weeks of implantation.

To compare the levels of the osteoblast markers in the new tissue samples from the different groups, the expression of the pre-osteoblastic marker Runx-2 [34], osteoblast marker OPN were analyzed by immunofluorescence staining. At 8 weeks post operation, the pre-osteoblastic marker Runx-2 was not expressed in the control group and the HLC group, whereas Runx-2 was found in the HLC-hBMP2 group (Fig. 6a). The osteoblast marker OPN was not expressed in the control group, but in both the HLC group and the HLC-hBMP2 group (Fig. 6a), yet the expression of OPN in the HLC group (3.87 ± 1.45%, n=4) was significantly less than that in the HLC-hBMP2 group (9.58 ± 2.81%, *$p < 0.05$, n=4, Fig. 6b). These results suggested that the HLC-hBMP2 significantly improved bone repairing.
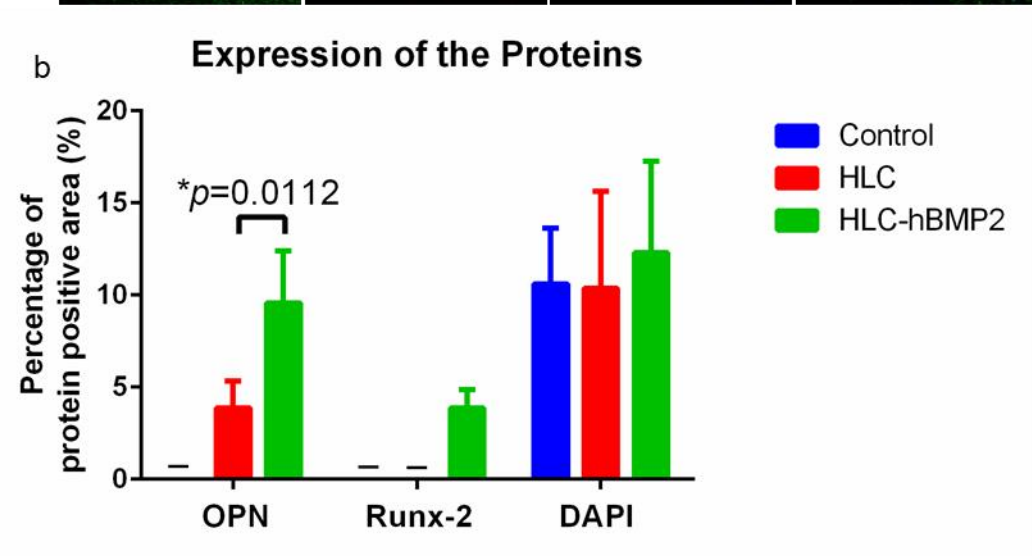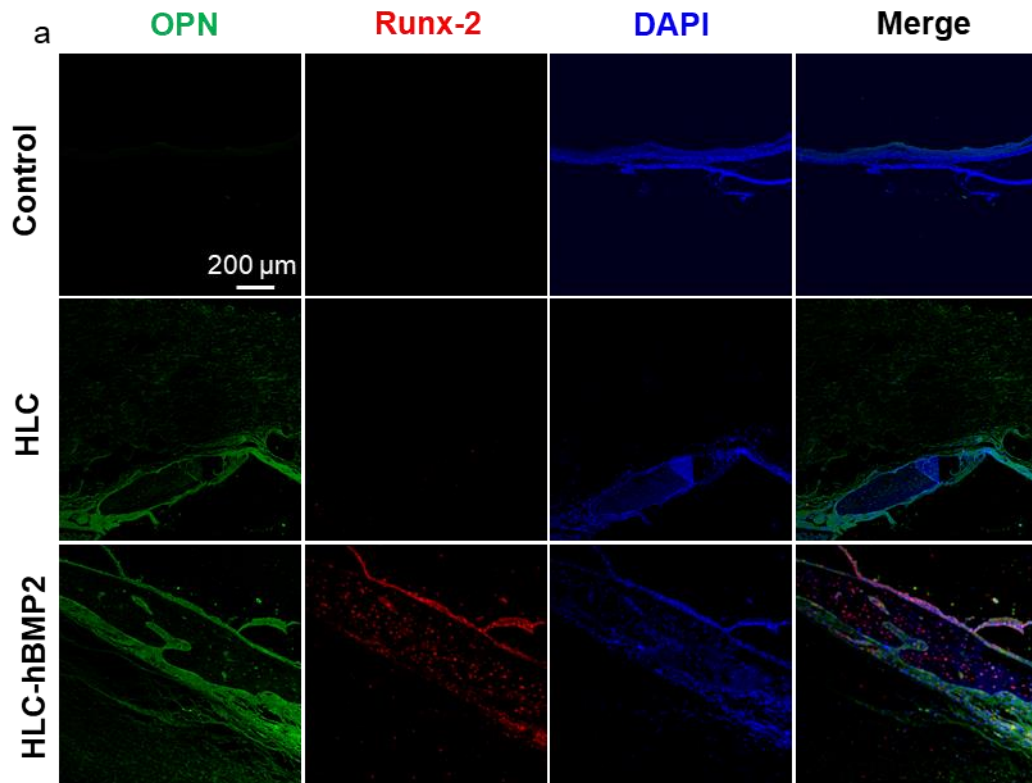
Fig. 6. Immunofluorescence analysis of the expression of bone marker proteins in the newly formed tissues from rat skull with standard aperture defect at 8 weeks post-operation. (a) Tissue sections of the HLC group and HLC-hBMP2 group were immunofluorescent stained with antibodies to OPN and Runx-2 bone marker proteins respectively, DAPI stained with blue, OPN protein labeled with green fluorescence while Runx-2 protein with red fluorescence. (b) Quantitative analysis of OPN and Runx-2 expression in each group (**p<0.01, n=4).

3.6.4 Histological evaluation of HLC-hBMP2 fusion protein degraded and released hBMP2 in vivo

In order to verify that HLC-hBMP2 fusion protein degraded and released hBMP-2 *in vivo*, the presence of BMP-2 in new bone tissue was detected by immunofluorescence. The primary antibody used was anti-BMP-2 antibody (host: rabbit, Abcam, ab14933), the secondary antibody used was goat anti-rabbit antibody (Alexa Fluor® 488-conjugated, Jackson, Lot: 137875), and the samples were stained with DAPI. In the end, photographs were taken with a laser confocal microscope (FV1000; Olympus Corporation, Tokyo, Japan). As shown in Fig. 7, after the implantation of the HLC-hBMP2 material for 8 weeks, hBMP2 ($2.93 \pm 2.12\%$, n=4) aggregated on one side of the new bone near the rat brain tissue, which confirmed that hBMP2 released after HLC degradation in the HLC-hBMP2. In particular, the HLC group also formed a small amount of bone tissue in the defect (Fig. 5-6), but hBMP2 was not detected in this bone tissue (Fig. 7), which further confirmed that hBMP2 in the HLC-hBMP2 group was not produced by the body itself but was released by material degradation. In addition, except for the surrounding of the new form tissue, we didn't detect the BMP-2 existing in the blood or other tissues of the rats. This may be due to the very low dose of BMP-2 released from the HLC-hBMP2 fusion protein and indirectly proved a controlled release of our novel device.
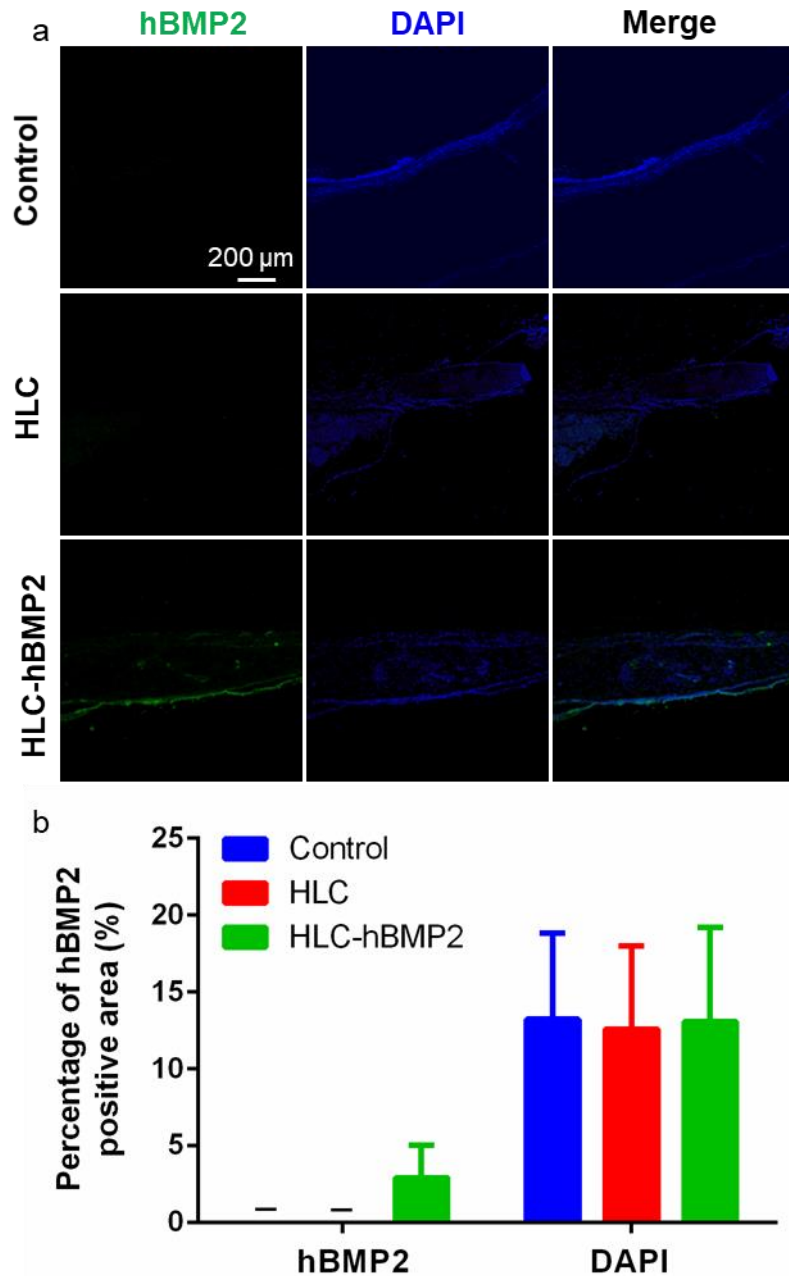
Fig. 7. Immunofluorescence analysis of hBMP2 expression in the newly formed tissues from rat skull with standard aperture defect at 8 weeks post operation. (a) Tissue sections of the HLC group and the HLC-hBMP2 group were immunofluorescent stained with hBMP2 antibody. The nucleus was stained blue by DAPI and hBMP2 was labeled with green fluorescence. (b) Quantitative analysis of hBMP2 in each group (n=4).

4. Discussion

There are normally two ways to improve the potency and efficacy of BMPs in bone repairing. One way is to modify BMPs as a dimer structurally or to use point mutants with improved properties [35-38]. Another way is to introduce carriers with optimized material and structural properties to optimize BMP retention and to improve BMP presentation to responding cells [39].

In this study, we took the second route to create the HLC-hBMP2 fusion protein scaffold which showed a different microstructure from the HLC scaffold after constructed by the gradient vacuum freeze-drying method. The HLC scaffold had a layered porous structure, while the HLC-hBMP2 scaffold presented with an omnidirectional through-hole structure (Fig. 2m, n). The elastic modulus of the HLC-hBMP2 scaffold with omnidirectional through-hole structure was markedly higher than that of the HLC scaffold, and thus improved its mechanical properties (Fig. 3a, b). Moreover, this vertical through-hole structure was beneficial for facilitating the migration of MSCs into the HLC-hBMP2 fusion material, and therefore HLC-hBMP2 enhanced MSCs migration (Fig. 4d).

In addition, HLC-hBMP2 showed stronger bone defect repairing ability *in vivo* than HLC alone. Eight weeks after the implantation of the two scaffolds into the cranial defect site in the rats, the bone defect repairing rate of the HLC-hBMP2 group (51.72 ± 16.68%, n=4) was significantly higher than that of the HLC group (21.01 ± 14.11%, $p<0.05$, n=4) and the control group (13.63 ± 3.62%, $p<0.01$, n=4, Fig. 5). These results demonstrated HLC-hBMP2 can successfully repair large size bone defects. In addition, there was no inflammatory reaction and infection during this repairing process.

The results from *in vitro* assays showed that HLC and HLC-hBMP2 had no significantly different effects on cell adhesion and proliferation (Fig. 4 and Fig. S4), confirming that HLC-hBMP2 fusion protein had no osteoinductive activity *in vitro*. The reason for this is that hBMP-2 can play a role in osteolysis only through forming a

dimer [3, 40], either heterodimeric BMPs or homodimeric BMP chimeras [35-38]. The reason why HLC-hBMP2 in this study did not form a dimer *in vitro* was due to the fact that HLC with a large molecular weight was attached to the C-terminus of hBMP-2 and made it impossible to form the dimer (Fig. 1). Yet, the results from *in vivo* assays revealed that the HLC-hBMP2 fusion protein can exert osteoinductive function and promoted the bone repairing rate to $51.72 \pm 16.68\%$ compared to the control group ($13.63 \pm 3.62\%$, p<0.01, n=4, Fig. 5-7) after implantation for 8 weeks. Actually, studies have shown that BMP signaling is complex *in vivo* due to the complicated dimer nature of the BMP ligands involved in signal transduction [35, 41, 42]. Besides, the role of potential responding cells in bone repairing from the periosteum, bone marrow, muscle/fascia, and vasculature may play a role although this role still remains unclear [43]. Therefore, it is crucial to determine the exact role of BMP-2 not only *in vitro* but also in the complex internal environment. The repairing effects for the period of 8 weeks implant was particularly evaluated in this study. This was based on our previous work [29] on the BMP2 release profile and for the comparison purpose. The traumatic bone animal model won't automatically repair within 8 weeks but can be reasonably repaired with purposely designed implants. The longitudinal and cross sections evaluation of the release of implants for bone repairing at different time scale in the future certainly would help to utilize the efficiency of this fused protein.

In our study, enzymatic degradation was used as an accelerated measurement of material degradation. Most of the HLC-hBMP2 were degraded in the Type I collagenase solution within 4 hours *in vitro* (Fig. 3e, f). Combined with *in vivo* assays, we inferred that the HLC in the HLC-hBMP2 fusion protein was enzymatically degraded slowly within 8 weeks. This was based on the observation of a significantly different amount of Col I detected in the newly formed tissues from all three groups (Fig. 5e). In addition, hBMP2 aggregated on one side of the new bone near the rat brain tissue after the implantation of the HLC-hBMP2 material for 8 weeks but it was not detected in the new bone from the HLC group. This further confirmed that hBMP2 was released from HLC-hBMP2 after the HLC degradation *in vivo* (Fig. 7).

In our previous study, the HLC sponge (linked through TG) was used as a delivery system to release hBMP-2 [29]. HLC sponge containing 5μg hBMP-2 released 15.03 ± 3.92% of hBMP-2 at day 1, 18.61 ± 2.61% at day 2 and 48.19 ± 8.69% at day 28. The HLC sponge containing 1μg hBMP-2 released 9.74 ± 1.56% at day 1, 18.13 ± 2.34% at day 3, and 44.79 ± 10.43% at day 28 [29]. In the current study, we did the same assays for hBMP2 release from the HLC-hBMP2 fusion scaffold *in vitro* using the same immersion solution (PBS), time points (1, 2, 3, 5, 7, 14, 21 and 28 days) and ELISA kit (Human BMP2 ELISA Kit, Abcam, ab119581, Lot GR3174552-1). However, the dose of released hBMP-2 was very low and barely detectable *in vitro* (data not shown). Perhaps it couldn't be released from the HLC-hBMP2 fusion scaffold due to the collagenase not present *in vitro* but only can be slowly released *in vivo* where collagenase was presented. But verification and measurement of hBMP2 release from fused protein *in vivo* turned out to be very challenging and we are not able to claim how exactly this release was achieved in the present study (data not shown and see discussion below). Nevertheless, our results showed that the fused HLC-hBMP2 improved bone regeneration.

Based on the above, we speculated that accompanying with the HLC degradation, the hBMP-2 can be controllably released and may form a dimer *in vivo* and then exert its osteogenic activity. As shown in Fig. 8, the HLC from the HLC-hBMP2 fusion protein was slowly hydrolyzed *in vivo*, which suggested a delayed process of releasing hBMP-2, and this in turn resulted in a stable release and better efficacy of hBMP-2 in bone repairing (Fig. 5-8). This result was different from our previous work which HLC sponge loaded with hBMP-2 for the rat cranial defect repair [29]. The HLC sponge loaded with hBMP-2 introduced rapid release but serious bone overgrowth occurred after implantation when loaded with a high dose of hBMP-2 (*i.e.* 5μg) [29]. These were also reflected in the measurements of osteoblast differentiation markers (Preosteoblast marker: Runx-2; Osteoblast marker: OPN) in repaired tissue correspondingly (Fig.8 in [29]).
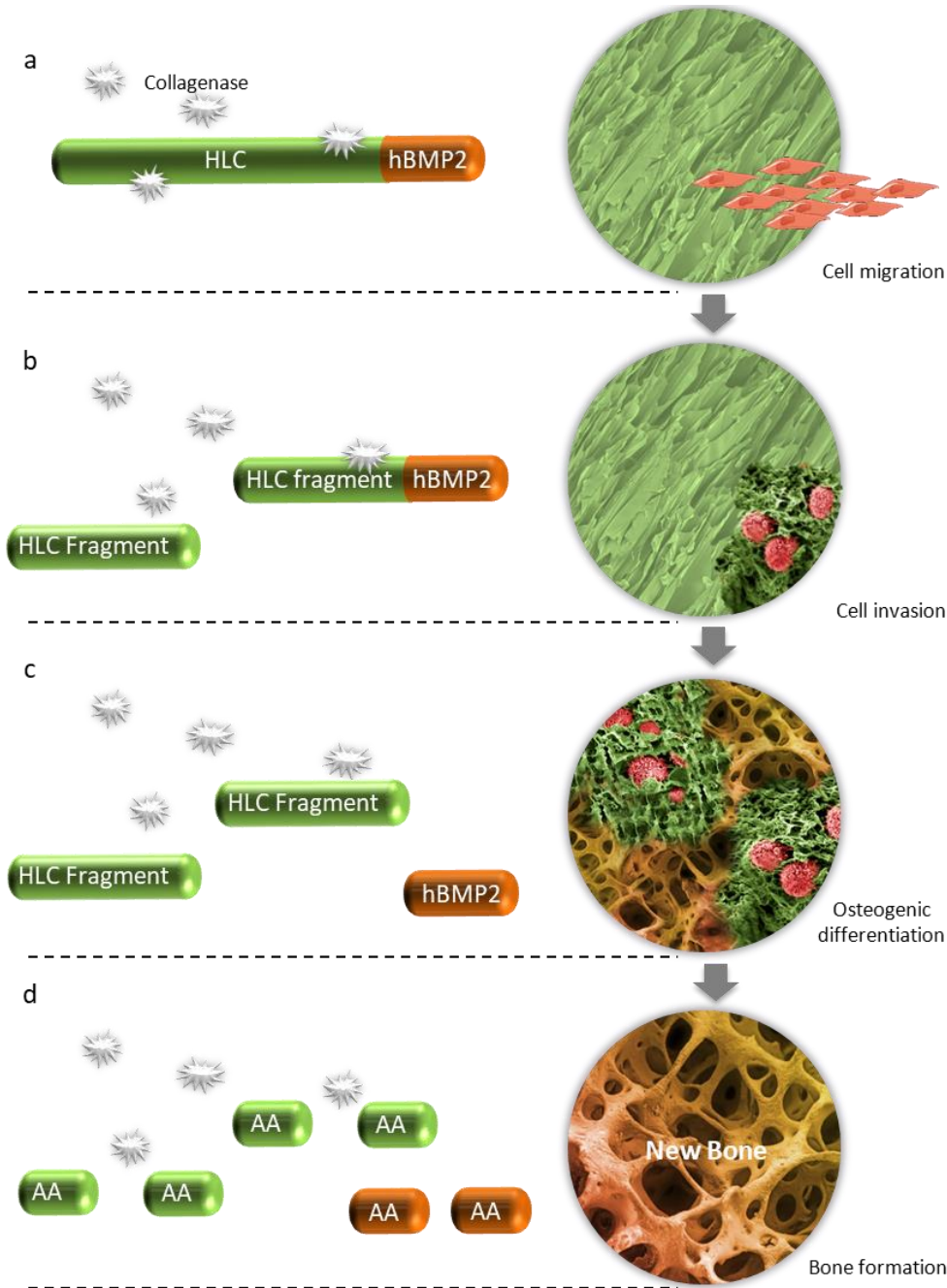
Fig. 8. Sketch of bone formation accompanied with hBMP2 release. (a) The vertical through-hole structure of HLC-hBMP2 enhanced cell migration into the scaffold; (b) Cell invaded and settled in the porous scaffold accompanied with HLC being degraded by Collagenase from the HLC-hBMP2 *in vivo*. (c) HLC was degraded and hBMP-2 was released from the HLC-hBMP2. The hBMP-2 formed dimer which improved osteogenic differentiation of cells. (d) The new bone formed and the HLC-hBMP2 was finally enzymatically degraded into amino acid (AA).

Compared with this previous work, the slow release of hBMP-2 from the HLC-hBMP2 fusion protein accompanying with the collagenase degradation *in vivo* achieved in this study was beneficial for a gentler and safer osteogenesis. We speculate that the unique structure of HLC-hBMP2 fusion protein may contribute to this, *i.e.* the HLC-hBMP2 fusion protein structure helped the stability of BMP2 or retained in the fusion protein; active BMP-2 was then sustained and controlled releas from the fusion through enzymatic degradation *in vivo*. The spatial and temporal control of the hBMP-2 release from the HLC-hBMP2 fusion protein in the bone defect repairing can be further achieved by designing a degradable linker between the HLC and the hBMP-2. The function of this linker is to controllably degrade in a specific internal environment and then release the hBMP-2 from the HLC-linker-hBMP2. The exact design of this linker could be a disulfide bonder (LEAGCKNFFPR↓SFTSCGSLE) to be inserted into a thrombin-sensitive sequence, a disulfide to be inserted into a protease-sensitive sequence, a dithiocyclic peptide linker (CRRRRRR↓EAEEAC) inserting protease sensitive sequence, etc. Through using the degradable linker and adjusting the localized microenvironment at the same time, such as adjusting the localized concentration of proteases, the hBMP-2 release could be further controlled to improve its efficacy in bone repairing.

The idea of using fusion protein as a delivery vehicle to effectively control the release of growth factors have been reported but mainly on the skin defects repairing [44-49]. However, fusion protein has not been applied in bone defect repairing, apart from one study using Elastin-like-polypeptide [50]. In this study, we successfully designed the HLC-hBMP2 fusion protein and used it to repair the bone defect for the first time. The construction of the HLC-hBMP2 fusion protein in our study had several advantages. Firstly, the HLC-hBMP2 fusion protein was a direct product, and this avoided the inactivation of hBMP-2 in the process of complexing with the HLC and therefore retained its stable osteogenic activity; Secondly, the designed HLC gene code in the HLC-hBMP2 fusion protein can be modified and controlled, and this resulted in a unique vertical through-hole structure of HLC-hBMP2 with the larger elastic modulus

(Fig. 2-3), a slow HLC degradation accompanying with the hBMP-2 stable release (Fig. 5-8), and some enhanced properties compared to animal tissue-extracted collagens when loaded with BMP-2 (Table S3). Thirdly, because the gene code in the HLC-hBMP2 was originated from the human gene code, the recombinant HLC-hBMP2 fusion protein produced thus had little potential virus risk and immunogenicity. In *in vivo* study, rats in all groups survived throughout the experiments, and there were no visible inflammatory reactions, infections or extrusions around the implantation sites observed, and there was none of the inflammatory cell infiltration shown in the supplementary images at high magnification (Fig. S5-7). Immunofluorescence staining also indicated that no CD206+ macrophages existed in the newly formed tissues after implantation 8 weeks (Fig. S11). All these indicated good biocompatibility of the scaffolds. Fourthly, the fused HLC-hBMP2 has no side effects and proved to be safer than other previous HLC-hBMP2 delivery systems (*i.e.* absorbing through TG links, Fig. 8 in [29]). All these proved that the HLC-hBMP2 had osteoinductive activity and promoted bone healing better than the traditional simple superposition of the hBMP-2/collagen sponge would do.

5. Conclusions

In this study, we constructed a novel HLC-hBMP2 fusion protein and successfully applied it in the bone repairing for the first time. This novel HLC-hBMP2 fusion protein formed a vertical through-hole structure with a larger elastic modulus compared with that of the HLC only scaffold. This unique structure of the HLC-hBMP2 scaffold facilitated the migration of MSCs into the material and the delivery of nutrients through the hole. As a novel delivery system for hBMP2, the HLC-hBMP2 fusion protein can controllably release hBMP-2 *in vivo* and thus have the stable osteogenic activity to promote healing of the rat cranial large size defect. Besides, this recombinant HLC-hBMP2 had little potential virus risk and immunogenicity compared with the normal commercial collagen sponges extracted from the animal tissues. Therefore, this novel recombinant fusion protein could be more beneficial in the treatment of bone defects

than the simple superposition of the hBMP2/collagen sponge. In addition, the method developed in this study to create the fusion protein overcame the high product costs and could be readily extended to produce other growth factors or therapeutic proteins. Furthermore, the design of the linker between HLC and hBMP-2 would contribute to achieving the spatial and temporal control of the HLC-hBMP2 fusion protein in the completion of bone defect repairing.

Supplementary data

Sequence 1: HLC gene sequence (1251 bp).

Sequence 2: GGGGS- hBMP2 gene sequence (385 bp).

Fig. S1: Sequencing result of the constructed pPIC9K-HLC-hBMP2 plasmid.

Fig. S2: PCR result of the yeast strain extracting genome.

Fig. S3: The N-terminal sequencing result of the HLC-hBMP2 fusion protein.

Fig. S4: Adhesion, proliferation and migration of rabbit MSCs on the HLC and the HLC-hBMP2 materials.

Fig. S5: H&E staining of the control sample at high magnification.

Fig. S6: H&E staining of HLC sample at high magnification.

Fig. S7: H&E staining of HLC-hBMP2 sample at high magnification.

Fig. S8: MTC staining of the control sample at high magnification.

Fig. S9: MTC staining of HLC sample at high magnification.

Fig. S10: MTC staining of HLC-hBMP2 sample at high magnification.

Fig. S11: Immunofluorescence analysis of CD206 in the newly formed tissues from rat skull with standard aperture defect at 8 weeks post operation.

Table S1: Culture conditions and culture media in the fermentor.

Table S2: The raw data of the swelling rate stability test for the HLC and HLC-hBMP2.

Table S3: Comparison between the commercial collagen sponges loaded with BMP-2 and the recombinant HLC-hBMP2 fusion materials.

Declaration of conflicting of interests

The authors declare no conflict of interest.

Acknowledgements

ORCID iDs

Zhuoyue Chen http://orcid.org/0000-0003-0590-2401

Lijun Shang http://orcid.org/0000-0001-5925-5903

Daidi Fan http://orcid.org/0000-0001-9798-1674

Fulin Chen http://orcid.org/0000-0001-9956-7194

Reference

[1] B. Poon, T. Kha, S. Tran, C.R. Dass, Bone morphogenetic protein-2 and bone therapy: successes and pitfalls. Journal of Pharmacy & Pharmacology 68(2) (2016) 139.

[2] U. Ripamonti, R. Duarte, R. Parak, C. Dickens, T. Dix-Peek, R.M. Klar, Redundancy and Molecular Evolution: The Rapid Induction of Bone Formation by the Mammalian Transforming Growth Factor-β3 Isoform. FRONT PHYSIOL 7 (2016) 396.

[3] Z. Sheikh, M.A. Javaid, N. Hamdan, R. Hashmi, Bone Regeneration Using Bone Morphogenetic Proteins and Various Biomaterial Carriers. MATERIALS 8(4) (2015) 1778-1816.

[4] S. Saini, A.J. Duraisamy, S. Bayen, P. Vats, S.B. Singh, Role of BMP7 in appetite regulation, adipogenesis, and energy expenditure. ENDOCRINE 48(2) (2015) 405-409.

[5] D. Katanec, M. Granic, M. Majstorovic, Z. Trampus, D.G. Panduric, Use of recombinant human bone morphogenetic protein (rhBMP2) in bilateral alveolar ridge augmentation: case report. Coll Antropol 38(1) (2014) 325-330.

[6] C. Bibbo, J. Nelson, D. Ehrlich, B. Rougeux, Bone morphogenetic proteins: indications and uses. Clin Podiatr Med Surg 32(1) (2015) 35-43.

[7] I. El Bialy, W. Jiskoot, M. Reza Nejadnik, Formulation, Delivery and Stability of Bone Morphogenetic Proteins for Effective Bone Regeneration. PHARM RES-DORDR 34(6) (2017) 1152-1170.

[8] I. Brigaud, R. Agniel, J. Leroy-Dudal, S. Kellouche, A. Ponche, T. Bouceba, N. Mihailescu, M. Sopronyi, E. Viguier, C. Ristoscu, F. Sima, I.N. Mihailescu, A.C.O. Carreira, M.C. Sogayar, O. Gallet, K. Anselme, Synergistic effects of BMP-2, BMP-6 or BMP-7 with human plasma fibronectin onto hydroxyapatite coatings: A comparative study. ACTA BIOMATER 55 (2017) 481-492.

[9] G.H. Lee, P. Makkar, K. Paul, B. Lee, Development of BMP-2 immobilized polydopamine mediated multichannelled biphasic calcium phosphate granules for improved bone regeneration. MATER LETT 208 (2017) 122-125.

[10] Z.Y. Chen, Z. Zhang, J.T. Feng, Y.Y. Guo, Y. Yu, J.H. Cui, H.M. Li, L.J. Shang, The influence of Mussel-Derived Bioactive BMP-2 decorated PLA on MSCs behavior in vitro and verification with osteogenicity at ectopic sites in vivo. ACS APPL MATER INTER 10 (2018) 11961-11971.

[11] S.S. Lee, B.J. Huang, S.R. Kaltz, S. Sur, C.J. Newcomb, S.R. Stock, R.N. Shah, S.I. Stupp, Bone regeneration with low dose BMP-2 amplified by biomimetic supramolecular nanofibers within collagen scaffolds. BIOMATERIALS 34(2) (2013) 452-459.

[12] L.B. Priddy, O. Chaudhuri, H.Y. Stevens, L. Krishnan, B.A. Uhrig, N.J. Willett, R.E. Guldberg, Oxidized alginate hydrogels for BMP-2 delivery in long bone defects. ACTA BIOMATER 10(10) (2014) 4390-4399.

[13] Q. Min, X. Yu, J. Liu, J. Wu, Y. Wan, Chitosan-Based Hydrogels Embedded with Hyaluronic Acid Complex Nanoparticles for Controlled Delivery of Bone Morphogenetic Protein-2. Pharmaceutics 11(5) (2019) 214.

[14] J. Wu, L. Li, C. Fu, F. Yang, Z. Jiao, X. Shi, Y. Ito, Z. Wang, Q. Liu, P. Zhang, Micro-porous polyetheretherketone implants decorated with BMP-2 via phosphorylated gelatin coating for enhancing cell adhesion and osteogenic differentiation. Colloids and Surfaces B: Biointerfaces 169 (2018) 233-241.

[15] M. Yamamoto, A. Hokugo, Y. Takahashi, T. Nakano, M. Hiraoka, Y. Tabata, Combination of BMP-2-releasing gelatin/β-TCP sponges with autologous bone marrow for bone regeneration of X-ray-irradiated rabbit ulnar defects. BIOMATERIALS 56 (2015) 18-25.

[16] Z. Wang, Z. Wang, W.W. Lu, W. Zhen, D. Yang, S. Peng, Novel biomaterial strategies for controlled growth factor delivery for biomedical applications. NPG ASIA MATER 9(10) (2017) 435.

[17] E. Lee, H. Lim, J. Hong, J. Lee, U. Jung, S. Choi, Bone regenerative efficacy of biphasic calcium phosphate collagen composite as a carrier of rhBMP-2. CLIN ORAL IMPLAN RES 27(11) (2016) 91-99.

[18] H. Lu, N. Kawazoe, T. Kitajima, Y. Myoken, M. Tomita, A. Umezawa, G. Chen, Y. Ito, Spatial immobilization of bone morphogenetic protein-4 in a collagen-PLGA hybrid scaffold for enhanced osteoinductivity. BIOMATERIALS 33(26) (2012) 6140-6146.

[19] G. Bhakta, Z.X.H. Lim, B. Rai, T. Lin, J.H. Hui, G.D. Prestwich, A.J.V. Wijnen, V. Nurcombe, S.M. Cool, The influence of collagen and hyaluronan matrices on the delivery and bioactivity of bone morphogenetic protein-2 and ectopic bone formation. ACTA BIOMATER 9(11) (2013) 9098-9106.

[20] J. Zhao, M. Shinkai, T. Takezawa, S. Ohba, U. Chung, T. Nagamune, Bone regeneration using collagen type I vitrigel with bone morphogenetic protein-2. J BIOSCI BIOENG 107(3) (2009) 318-323.

[21] R.J. Mannion, A.M. Nowitzke, M.J. Wood, Promoting fusion in minimally invasive lumbar interbody stabilization with low-dose bone morphogenic protein-2--but what is the cost? Spine Journal Official Journal of the North American Spine Society 11(11) (2011) 527-533.

[22] M. Miyazaki, Y. Morishita, W. He, M. Hu, C. Sintuu, H.J. Hymanson, J. Falakassa, H. Tsumura, J.C. Wang, A porcine collagen-derived matrix as a carrier for recombinant human bone morphogenetic protein-2 enhances spinal fusion in rats. The Spine Journal 9(1) (2008) 22-30.

[23] B. Chen, H. Lin, J. Wang, Y. Zhao, B. Wang, W. Zhao, W. Sun, J. Dai, Homogeneous osteogenesis and bone regeneration by demineralized bone matrix loading with collagen-targeting bone morphogenetic protein-2. BIOMATERIALS 28(6) (2007) 1027-1035.

[24] M.S. Kumar, S. Kirubanandan, R. Sripriya, P.K. Sehgal, Triphala incorporated collagen sponge--a smart biomaterial for infected dermal wound healing. J SURG RES 158(1) (2010) 162.

[25] H. Begam, S.K. Nandi, B. Kundu, A. Chanda, Strategies for delivering bone morphogenetic protein for bone healing. Mater Sci Eng C 70(1) (2017) 856-869.

[26] X. Jiang, Y. Wang, D. Fan, C. Zhu, L. Liu, Z. Duan, A novel human-like collagen hemostatic sponge with uniform morphology, good biodegradability and biocompatibility. J BIOMATER APPL 31(8) (2017) 1099-1107.

[27] L. Zhao, L. Xian, J. Zhao, S. Ma, X. Ma, D. Fan, C. Zhu, Y. Liu, A novel smart injectable hydrogel prepared by microbial transglutaminase and human-like collagen: Its characterization and biocompatibility. Materials Science & Engineering C 68 (2016) 317-326.

[28] C. Zhu, D. Fan, Y. Wang, Human-like collagen/hyaluronic acid 3D scaffolds for vascular tissue engineering. Materials Science & Engineering C 34(1) (2014) 393-401.

[29] Z. Chen, Z. Zhang, X. Ma, Z. Duan, J. Hui, C. Zhu, D. Zhang, D. Fan, L. Shang, F. Chen, Newly Designed Human-like Collagen to Maximize Sensitive Release of BMP-2 for Remarkable Repairing of Bone Defect. Biomolecules 9(9) (2019) 450.

[30] P.A. Parmar, S.C. Skaalure, L.W. Chow, J.P. St-Pierre, V. Stoichevska, Y.Y. Peng, J.A. Werkmeister, J.A. Ramshaw, M.M. Stevens, Temporally degradable collagen-mimetic hydrogels tuned to chondrogenesis of human mesenchymal stem cells. BIOMATERIALS 99 (2016) 56-71.

[31] A.H. Morris, D.K. Stamer, B. Kunkemoeller, J. Chang, H. Xing, T.R. Kyriakides, Decellularized materials derived from TSP2-KO mice promote enhanced neovascularization and integration in diabetic wounds. BIOMATERIALS 169 (2018) 61-71.

[32] Z. Chen, J. Wei, J. Zhu, W. Liu, J. Cui, H. Li, F. Chen, Chm-1 gene-modified bone marrow mesenchymal stem cells maintain the chondrogenic   phenotype of tissue-engineered cartilage. STEM CELL RES THER 7(1) (2016) 70.

[33] Z. Chen, S. Yue, Z. Jing, L. Wei, J. Cui, H. Li, F. Chen, Laminated electrospun nHA/PHB-composite scaffolds mimicking bone extracellular matrix for bone tissue engineering. Mater Sci Eng C Mater Biol Appl 72 (2017) 341-351.

[34] F. Knopf, C. Hammond, A. Chekuru, T. Kurth, S. Hans, C.W. Weber, G. Mahatma, S. Fisher, M. Brand, S. Schulte-Merker, G. Weidinger, Bone regenerates via dedifferentiation of osteoblasts in the zebrafish fin. DEV CELL 20(5) (2011) 713-724.

[35] D. Yadin, P. Knaus, T.D. Mueller, Structural insights into BMP receptors: Specificity, activation and inhibition. CYTOKINE GROWTH F R 27 (2016) 13-34.

[36] K. Schmidt-Bleek, B.M. Willie, P. Schwabe, P. Seemann, G.N. Duda, BMPs in bone regeneration: Less is more effective, a paradigm-shift. CYTOKINE GROWTH F R 27 (2016) 141-148.

[37] J.W. Lowery, B. Brookshire, V. Rosen, A Survey of Strategies to Modulate the Bone Morphogenetic Protein Signaling Pathway: Current and Future Perspectives. STEM CELLS INT 2016(30) (2016) 1-15.

[38] Y. Byung-Hak, E. Luis, A. Chihoon, P.C. Gray, Y. Sang-Kyu, K. Witek, C. Senyon, An activin A/BMP2 chimera, AB204, displays bone-healing properties superior to those of BMP2. Journal of Bone & Mineral Research 29(9) (2015) 1950-1959.

[39] E. Migliorini, A. Valat, C. Picart, E.A. Cavalcanti-Adam, Tuning cellular responses to BMP-2 with material surfaces. CYTOKINE GROWTH F R 27 (2016) 43-54.

[40] J.M. Granjeiro, R.C. Oliveira, J.C. Bustos-Valenzuela, M.C. Sogayar, R. Taga, Bone morphogenetic proteins: from structure to clinical use. Brazilian Journal of Medical & Biological Research 38(10) (2005) 1463-1473.

[41] H. Kai, A. Seher, W. Schmitz, T.D. Mueller, W. Sebald, J. Nickel, Receptor oligomerization and beyond: a case study in bone morphogenetic proteins. BMC Biology,7,1(2009-09-07) 7(1) (2009) 59.

[42] M.J. Isaacs, Y. Kawakami, G.P. Allendorph, B.H. Yoon, J.C.I. Belmonte, S. Choe, Bone

morphogenetic protein-2 and -6 heterodimer illustrates the nature of ligand-receptor assembly. MOL ENDOCRINOL 24(7) (2010) 1469-1477.

[43] H.J. Seeherman, S.P. Berasi, C.T. Brown, R.X. Martinez, Z.S. Juo, S. Jelinsky, M.J. Cain, J. Grode, K.E. Tumelty, M. Bohner, O. Grinberg, N. Orr, O. Shoseyov, J. Eyckmans, C. Chen, P.R. Morales, C.G. Wilson, E.J. Vanderploeg, J.M. Wozney, A BMP/activin A chimera is superior to native BMPs and induces bone repair in nonhuman primates when delivered in a composite matrix. SCI TRANSL MED 11(489) (2019) 1-20.

[44] I. Elloumi, R. Kobayashi, H. Funabashi, M. Mie, E. Kobatake, Construction of epidermal growth factor fusion protein with cell adhesive activity. BIOMATERIALS 27(18) (2006) 3451-3458.

[45] P. Koria, H. Yagi, Y. Kitagawa, Z. Megeed, Y. Nahmias, R. Sheridan, M.L. Yarmush, Self-assembling elastin-like peptides growth factor chimeric nanoparticles for the treatment of chronic wounds. P NATL ACAD SCI USA 108(3) (2011) 1034-1039.

[46] A. Yeboah, The use of stromal cell derived growth factor 1-elastin like peptide fusion protein nanoparticles to improve chronic skin wounds. Ph.D. Dissertation (2016).

[47] A. Yeboah, T. Maguire, R. Schloss, F. Berthiaume, M.L. Yarmush, Stromal Cell-Derived Growth Factor-1 Alpha-Elastin Like Peptide Fusion Protein Promotes Cell Migration and Revascularization of Experimental Wounds in Diabetic Mice. ADV WOUND CARE 6(1) (2017) 10-22.

[48] J. Yang, W. Qiang, S. Ren, S. Yi, J. Li, L. Guan, L. Du, Y. Guo, H. Hu, H. Li, High-efficiency production of bioactive oleosin-basic fibroblast growth factor in A. thaliana   and evaluation of wound healing. GENE 639 (2017) 69-76.

[49] J. Cai, R. Wen, W. Li, X. Wang, H. Tian, S. Yi, L. Zhang, X. Li, C. Jiang, H. Li, Oil body bound oleosin-rhFGF9 fusion protein expressed in safflower (Carthamus tinctorius L.) stimulates hair growth and wound healing in mice. BMC BIOTECHNOL 18(1) (2018) 51.

[50] McCarthy B, Yuan Y, Koria P. Elastin-like-polypeptide based fusion proteins for osteogenic factor delivery in bone healing. BIOTECHNOL PROG. 32(4) (2016) 1029-1037.